THE L-TYPE VOLTAGE-GATED CALCIUM CHANNEL MODULATES MICROGLIAL PRO-INFLAMMATORY ACTIVITY

Espinosa-Parrilla* JF[1,3], Martínez-Moreno* M[1], Gasull X[2], Mahy N[1], Rodríguez MJ[1]

1. Unitat de Bioquímica i Biologia Molecular, Facultat de Medicina, Institut d'Investigacions Biomèdiques August Pi i Sunyer (IDIBAPS), Universitat de Barcelona, and Centro de Investigación Biomédica en Red sobre Enfermedades Neurodegenerativas (CIBERNED), Barcelona, Spain.

2. Laboratori de Neurofisiologia, Facultat de Medicina, IDIBAPS, Universitat de Barcelona, Barcelona, Spain

3. Current address: Neurotec Pharma SL, Bioincubadora PCB-Santander, Parc Científic de Barcelona, Barcelona, Spain

* JF Espinosa-Parrilla & M Martínez-Moreno contributed equally to this work

Author for correspondence: Dr. Manuel J. Rodríguez
Unitat de Bioquímica i Biologia Molecular
Facultat de Medicina, UB
c/ Casanova 143
E-08036 Barcelona, SPAIN
Phone: +34 93 402 0586
FAX: + 34 93 403 5882
e-mail: marodriguez@ub.edu

Running headline: L-type VGCC modulates microglial activity

ABSTRACT

Under pathological conditions, microglia, the resident CNS immune cells, become reactive and release pro-inflammatory cytokines and neurotoxic factors. We investigated whether this phenotypic switch includes changes in the expression of the L-type voltage-gated calcium channel (VGCC) in a rat model of N-methyl-D-Aspartate-induced hippocampal neurodegeneration. Double immunohistochemistry and confocal microscopy evidenced that activated microglia express the L-type VGCC. We then analyzed whether BV2 microglia express functional L-type VGCC, and investigated the latter's role in microglial cytokine release and phagocytic capacity. Activated BV2 microglia express the $Ca_V1.2$ and $Ca_V1.3$ subunits of the L-type VGCC determined by reverse transcription-polymerase chain reaction, Western blot and immunocytochemistry. Depolarization with KCl induced a Ca^{2+} entry facilitated by Bay k8644 and partially blocked with nifedipine, which also reduced TNF-α and NO release by 40%. However, no nifedipine effect on BV2 microglia viability or phagocytic capacity was observed. Our results suggest that in CNS inflammatory processes, the L-type VGCC plays a specific role in the control of microglial secretory activity.

KEYWORDS: L-type voltage-gated calcium channel, excitotoxicity, dihydropyridine receptor, neuroinflammation, neurodegeneration.

Introduction

Microglial reaction is an early event which often precedes and triggers neuronal death in CNS pathological situations such as Alzheimer's and Parkinson's diseases, amyotrophic lateral sclerosis, multiple sclerosis, ischemia and brain trauma (Graeber and Streit, 2010). As a response to signals released during injury, this microglial transition from a surveillance state towards a more reactive one represents an important phenotypic change (Colton and Wilcock, 2010; Domercq et al., 2013; Kettenmann et al., 2011). As a result, reactive microglia releases pro-inflammatory cytokines and neurotoxic factors, such as tumor necrosis factor-α (TNF-α), interleukin-1β (IL-1β) and reactive oxygen species, the excessive production of which may trigger or exacerbate neuronal death (Liao et al., 2012; Zhang et al., 2011). In addition, some microglial cells become increasingly dysfunctional as they age, and may participate directly in the development of secondary tissue injury and neurodegeneration (Damani et al., 2011; Liao et al., 2012). Therefore, control of microglial activation should bring therapeutic benefit for any central disorder related with neuroinflammation. A growing body of evidence suggests that ion channels expressed by microglia are modulators of cell functions, and highlights their direct involvement in these neuropathologies (Kettenmann et al., 2011; Ortega et al., 2012a, 2013; Rodríguez et al., 2013; Virgili et al., 2011, 2014).

Electrophysiological studies suggest that microglia express a voltage-gated calcium channel (VGCC) which mediates Ca^{2+} entry (Colton et al., 1994; Hegg et al., 2000; Silei et al., 1999). Structurally, all VGCC family members are organized as heteromeric complexes of five subunits: α1, α2, β, δ, and γ (Zamponi and Snutch, 2013). The α1 subunit is the pore-forming component

and functions as the voltage sensor (Catterall et al., 2005). The heterogeneity of each subunit gives rise to different VGCC pharmacological and electrophysiological properties and to the classification of the P-, Q-, N-, L-, R-, and T-type channels (Catterall et al., 2005). The α_{1C} ($Ca_V1.2$) and α_{1D} ($Ca_V1.3$) genes encode the α1 subunit of the L-type Ca^{2+} channel, which was first recognized as essential for coupling excitation to contraction in skeletal, cardiac, and smooth muscle cells (Lipscombe et al., 2004). The L-type VGCC is also expressed in neurons and endocrine cells where it regulates a diversity of processes including neurohormone and transmitter secretion, gene expression, mRNA stability, synaptic efficacy, and the activity of other ion channels (Ashcroft et al., 1994; Bading et al., 1993; Bean, 1989).

The L-type VGCC, which has a role in neuronal survival and ischemia-induced axonal injury, is considered a target for therapies designed to interfere with neuropathological processes. Thus, L-type VGCC blockade with dihydropyridine or nimodipine reduces neuronal damage and improves behavioral outcome accompanied with excitotoxicity, traumatic brain injury and ischemia (Bernal et al., 2009; Mattsson et al., 1999; Zhu et al., 1999;). However, calcium antagonist treatments in hypoxia-ischemia models have an effectiveness of only 50% (Horn et al., 2001) and these same VGCC blockers present contradictory results in a large number of calcium-mediated excitotoxic processes (Berg et al., 1995; Bernal et al., 2009; Frandsen et al., 1993; Fryer et al., 1999; Horn et al., 2001; Petegnief et al., 2004; Rami and Krieglstein, 1994; Small et al., 1997). Inside this framework, the characterization of microglial expression of the L-typeVGCC after brain injury will help to establish why the channel blockade therapy remains so challenging in experimental and clinical assays.

In this paper we postulated that phenotypic activation of microglia during injury alters L-type VGCC expression, resulting in a modification of intracellular microglial events such as cytokine release and phagocytosis. We investigated activated microglia in our *in vivo* experimental model of neurodegeneration and in *in vitro* cultures of the BV2 microglial cell line. In our rodent model, N-methyl-D-aspartate (NMDA) is stereotaxicaly microinjected into the hippocampal formation to induce a neurodegenerative process involving neuronal necrosis and a potent inflammatory reaction mainly mediated by microglia (Ortega et al., 2012b; Rodríguez et al., 2013). BV2 cell culture allows the determination of the function of the L-type VGCC in microglia activity. Our results suggest a major role for the L-type VGCC in specifically controlling microglial pro-inflammatory activity in CNS pathologies.

Material and methods

Animals

Adult male Wistar rats (body weight 200-225 g at the beginning of the study) were obtained from the animal housing facilities of the School of Medicine at the University of Barcelona). They were kept on a 12 hours/12 hours day and night cycle, and housed with free access to food and water. Animals were handled in accordance with European legislation (86/609/EEC). All efforts were made to minimize the number of animals used and their suffering. The procedures were approved by the University of Barcelona's Ethics Committee under the supervision of the Catalan government.

Materials

Murine BV2 microglial cell line was purchased from Cell Bank (Interlab Cell Line Collection, ICLC, Geneva, Italy). RPMI medium supplemented with L-glutamine was purchased from GIBCO (USA). Fetal Bovine Serum, was from VWR Scientific (San Francisco, USA). All culture plaques and flasks were purchased from Nunc (Roskilde, Denmark). N-Methyl-D-Aspartate, lipopolysaccharide from *Escherichia coli* 026:B6 (LPS), interferon-gamma (IFNγ), Nifedipine, nimodipine, Bay k8644, the biotin-conjugated isolectin B4 (IB4) from *Bandeiraea simplifolia*, the mouse monoclonal anti-Glial fibrillary acidic protein (GFAP) antibody, peroxidase-conjugated IgG as secondary antibody, and the Extradivin-Cy3 conjugate were all from Sigma-Aldrich (St. Louis, CA). The polyclonal rabbit anti-α1C antibody was from Alomone Labs (Jerusalem, Israel). Goat anti-rabbit IgG antibody conjugated with Alexa-fluor 488, Goat anti-mouse IgG antibody conjugated with Alexa-fluor 555 and FluoSpheres Carboxylate-modified microspheres were from Invitrogen (Carlsbad, CA). The fura-2 acetoxymethyl ester was from Calbiochem (San Diego, CA).

Stereotaxic procedure and rat brain sample collection

Under equithesin anesthesia (a mixture of chloral hydrate and sodium pentobarbital; 0.3 ml/100g body wt., i.p.) eight rats were placed in a stereotaxic instrument (David Kopf, Carnegie Medicine, Sweden) with the incisor bar set at -3.3 mm. Following Paxinos and Watson's Atlas (Paxinos and Watson, 1986), the stereotaxic coordinates of the hippocampal microinjection were 3.3 mm caudal to bregma, 2.2 mm lateral to bregma and 2.9 mm ventral from dura. A 5.0 µl Hamilton syringe activated by an infusion pump (CMA/100; Carnegie Medicine, Sweden) was used for the intracerebral injection into the hippocampal parenchyma. All injections lasted 5 min. After onset of the infusion of 0.5 µl, the

needle was left in place for an additional 5 min to allow passive diffusion and to prevent spread of the excitotoxin up the cannula track upon removal; then, the needle was slowly retracted. Four animals received a single microinjection of 20 nmol NMDA in 50mM phosphate buffer saline (PBS; pH 7.4) (NMDA group n =4) or a single microinjection of 50mM PBS (pH 7.4) (sham group n = 4).
On day 15 post-lesion, rats were anaesthetized with equithesin and transcardially perfused with 300 ml of 0.01 M PBS followed by 300 ml of 4% (w/v) paraformaldehyde in 0.01 M PBS. Brains were then removed, post-fixed for 2 hours, and thereafter transferred to 15% (w/v) sucrose in PBS at 4ºC for three days. The brains were frozen with powdered dry ice and stored at -80ºC until use. Coronal serial 14 µm sections at the level of the injection site (3.3 mm caudal to bregma) were obtained and mounted on slices pretreated with poly-L-lysine (10% w/v in distilled water).

Histology, immunohistochemistry and confocal analysis

Standard Nissl staining of brain slices was performed to evaluate neuronal loss and the morphology of the hippocampal region. Microglial cells were identified by histochemistry with biotin-conjugated IB4 (Rodríguez et al., 2001). Briefly, sections were incubated overnight at 4 ºC with IB4 diluted 1:25 in normal goat serum (NGS, 1:100 v/v in 0.01 M PBS; pH 7.4). Immunohistochemistry was carried out in consecutive sections with the avidin-biotin peroxidase method as previously described (Rodríguez et al., 2009a). The L-type VGCC was labeled with polyclonal rabbit anti-α_{1C} antibody (1/200) in 3% NGS. After incubation with ExtrAvidin (1/250), sections were developed in a 0.05 M Tris solution containing 0.03% (w/v) diaminobenzidine (DAB) and 0.006% (v/v) H_2O_2. Finally, sections were dehydrated, cleared and mounted with DPX.

The hippocampal size and the area occupied by the neural loss were measured on Nissl stained sections using a computer-assisted image analysis system (Image-Pro Plus, Media Cybernetics Inc., MD, USA). Microglial reaction area was measured on IB4-stained sections using the same system. In both cases, the area of contralateral hippocampus was measured in the same sections in order to estimate the effects of histological procedures on tissue size, and thus to correct for variability in individual bain size and tissue shrinkage. Stereological counting was made on sections from NeuN single immunostaining or IB4 histochemistry. We applied the optical fractionator method to count labeled cells (Ortega et al., 2013). Lesioned regions of the hippocampal formation were outlined at 2.5x magnification on arbitrary uniform random (AUR) coronal sections. Individual cells were viewed at 40x in AUR-sampled sites chosen by the Mercator Pro 7.0 software (ExploraNova) and then counted. To determine the presence of L-type VGCC in microglia, double immunohistochemistry was performed with the polyclonal rabbit anti-α_{1C} antibody and IB4 (1/25) as a specific markers for microglia. 14 µm-thick adjacent sections were first incubated for 2 hours at room temperature in PBS containing 0.1% Triton X-100, 5% BSA and 5% NGS. Then, sections were co-incubated overnight at 4ºC with the anti-α1C antibody (1/200) and the IB4 (1/25). Antibodies against the IgG of appropriate species, conjugated with fluorescent dyes Alexa-fluor 488 (1/300) or Alexa-fluor 555 (1/300) Extravidin-Cy3 conjugate (1/500), were used to detect microglial cells. All sections were mounted in Pro-long antifade and kept in the dark. Incubations with either mouse or rabbit IgG as primary antibodies were used for negative controls. In each 14 µm-thick slice, series of 10 confocal images were acquired at x40 using

a Leica TCS SL laser scanning confocal spectral microscope (Z resolution = 586 nm; Leica Microsystems Heidelberg GmbH, Mannheim, Germany). Co-localization of fluorescent labelling in the hippocampus was analyzed in single confocal images by displaying the spatial distribution of normalized mean deviation product (MDP) values with an appropriate lookup table (Jaskolski et al., 2005) and by displaying the scatter plot of pixel distribution of each image. The co-localization study was performed as published elsewhere (Manders et al., 1993) and included the estimation of Pearson's r that describes the extent of overlap between image pairs and gives a value between -1 and 1, with -1 being no overlap whatsoever between images and 1 a perfect image registration. The Overlap coefficient R, which describes overlap independently from intensity image, and Overlap coeficients for green (k1) and red (k2) where also calculated. All image analyses were made with ImageJ 1.39u (National Institutes of Health, USA) and FluoColoc (ExploraNova, France) specific software. The number of cells showing double immunostaining was estimated by counting of cells on 3 random confocal photomicrographs (n = 60 cells/image). Results are given as a percentage of the total number of cells.

BV2 cell culture, immunocytochemistry and phagocytic assay

BV2 cells were cultured in RPMI 1640 medium with L-glutamine and supplemented with 10% (v/v) heat-inactivated fetal bovine serum (FBS), 100U/ml penicillin and 100 µg/ml streptomycin. Cells were grown in a humidifier cell incubator containing 5% CO_2 at 37ºC. Before activation, cells were sub-cultured on 24-well plates at a density of $5x10^4$ cells/ml for 24 hours, and plates were divided into 5 groups of cultured cells: a) One group with no further manipulation, called control; b) The C+Nif group, in which BV2 cells were

incubated with 10 μM Nifedipine 24h after sub-culture; c) the L+I group, in which BV2 cells were activated with lipopolysaccharide (LPS)+ interferon gamma (IFNγ) (0.1 μg/ml and 0.5 ng/ml) for 48 hours as described elsewhere (Ortega et al., 2012a), d) the L+I+Nif group, in which cells were incubated with 10 μM Nifedipine 24h after activation with LPS+ IFNγ and e) the L+I+Bayk group, in which cells were incubated with 10 μM Bay k8644 24h after activation with LPS+ IFNγ. 10μM Nifedipine was used for spacific pharmacological blockade of the L-type VGCC and 10μM Bay k8644 for specific openning of the channel. In some experiments, 25 μM Nimodipine was used to block L-type VGCC. 48 Forty-eight hours after activation, culture media were collected for further analysis and protein and mRNA purification was performed using the NucleoSpin® RNA/Protein kit (QUIAGEN, Düsseldorf, Germany) in accordance with the manufacturer's specifications.

For immunocytochemistry assays, BV2 cells were grown on poly-D-lysine-coated sterile coverslips and the medium was changed on the day of activation with LPS+IFNγ. At 48 hours, cells were fixed in ice-cold methanol for 8 minutes. Immunodetection was performed using anti- α1C (1/1000) primary antibody detected with Alexa-fluor 488 conjugated secondary antibody (1/500). Controls for non-specific binding were performed, excluding primary antibodies. Cell nuclei were stained with Hoechst33258 (2.5μg/ml in PBS). Coverslips were mounted with Pro-long Antifade and slices were stored at 4ºC. Images were acquired using a Zeiss Axio Observer Fluorescence Microscope (Göttingen, Germany).

For the study of the phagocytic capacity, cells were incubated for 30 minutes at 37ºC in the presence of 2μm diameter FluoroSpheres at 0.01% solid mass as

described previously by Ortega et al. (2012a). In parallel, immunofluorescence with anti-alpha-tubulin antibody conjugated with FITC was carried out for cell identification, as described above. Five images/well were acquired randomly using Zeiss Axio Observer Fluorescence Microscopy. Quantification was done in each picture with ImageJ, by counting the cells containing at least one fluorosphere.

Measurement of cytosolic-free Ca^{2+} and stimulation of VGCC

Intracellular calcium concentration ($[Ca^{2+}]_i$) was measured as described in detail previously (Bataller et al., 2001; Soto et al., 2004). Briefly, BV2 cells were plated on 25-mm diameter glass coverslips (VWR Scientific Inc., Philadelphia, PA) and then loaded with 4 μM fura-2/acetoxymethyl ester (Calbiochem, San Diego, CA) for 35 minutes at 37°C in an incubation buffer of 130 mM NaCl, 10 mM HEPES, 2.7 mM KCl, 1.2 mM 1.2 $MgCl_2$, 2.5 mM $CaCl_2$ and 10 mM glucose at pH 7.4 with NaOH. Fura-2-loaded BV2 microglia were then transferred into an open flow chamber mounted on the heated stage of an inverted epifluorescence microscope (Diaphot-300; Nikon, Tokyo, Japan) and maintained at 37°C. Examination of the fura-2 fluorescence distribution did not show significant intracellular heterogeneity. Fluorescence images were obtained at 40x by a charge-coupled device camera (CH250; Photometrics, Tucson, AZ) digitized, stored, and analyzed on a computer (Macintosh 840AV; Apple, Inc., Cupertino, CA). After a stabilization period of 10 min, image pairs were obtained alternately every 4 seconds, and, for a total of 12 minutes, at excitation wavelengths of 340 and 380 nm (10-nm bandwidth filters), to excite the Ca^{2+}-bound and Ca^{2+}-free forms of this ratiometric dye respectively. The emission wavelength was 510 nm (120-nm bandwidth filter) and $[Ca^{2+}]_i$ values were calculated on a single cell

basis by determining the 340- to 380-nm fluorescence (F_{340}/F_{380}) ratios at each time point. All images were checked for movement artifacts, and a reference point was used to obtain true co-registration of the 340-nm and 380-nm images. The opening of the VGCC was induced through cell membrane depolarization by addition of 80 mM KCl as previously described (Bataller et al., 2001). Osmolarity effects were controlled for using 50 to 150 mM NaCl. KCl addition was not associated with any change in cell viability, as assessed by trypan blue exclusion assay (Strober, 2001). Pharmacological blockade of the VGCC was performed by addition of 10μM Nifedipine to the incubation medium, and openning of the channel was induced by addition of 10μM Bay k8644 to the incubation medium. Cells were considered to be responders when $[Ca^{2+}]_i$ increased by more than 20% relative to the baseline level. Each condition was analized in cells from 3-7 different cultures.

RT-PCR analysis and Western blotting of $Ca_V1.2$ and $Ca_V1.3$ in BV2 cells

RT-PCR was performed to assess the presence of α1C mRNA inside BV2 cells. Total RNA from BV2 cells was isolated using NucleoSpin RNA/protein kit in accordance with the manufacturer's instructions (Macherey-Nagel, Germany). The concentration of total RNA isolated was quantified using a NanoDrop N1000 spectrophotometer (Thermo, Wilington, DE). Specific primers were designed against mouse mRNA sequences of the subunits α1C and α1D of the L-type VGCC as described previously (Toba et al., 2005). The sequences for α1C are: F 5'-TGCCTGGTGCTCGGGGTTTC-3'; R 5'-GGGGGTGGACCGCACCATTT-3' (GeneBank accession number: NM_009781). The sequences for α1D are: F 5'-GCACCGTGGTGTCCTGTGAATGC-3'; R 5'-

GGAAAGTGATGGGATGAGATCTC-3' (GeneBank accession number: AK018426). Sequence of 18S non-coding mRNA (GeneBank accession number: NR_003278.1) was used as control. RT reactions were carried out using random primers and 2 µg of mRNA as described by the manufacturer with AffinityScript Multiple Temperature cDNA Synthesis kit (Stratagene, CA). PCR was performed with the Taq PCR Core kit of Qiagen (Studio City, CA) using 2µl of RT reaction as a template. The cycling conditions were those described previously (Toba et al., 2005). For 18S mRNA, cycling conditions complied with the manufacturer's instructions, with the annealing temperature fixed at 57ºC. Appropriate templates were included as positive and negative controls. PCR products (10 µl) were separated by 1.5% agarose gel electrophoresis and visualized by staining with ethidium bromide.

Whole cell culture proteins and brain homogenates were obtained in RIPA buffer (Santa Cruz Biotechnology, Santa Cruz, CA) as described previously (Ortega et al., 2012a). The supernatant and the pellet were collected. Aliquots containing 20 µg protein were subjected to 10% SDS-PAGE. Proteins were transferred to Nitrocellulose membrane (Amersham Pharmacia Biotech, San Francisco, CA) and probed by incubation with anti-α_{1C} (1/200), as primary antibodies and with peroxidase-conjugated IgG (1/2500) as secondary antibody. Blots were visualized using the enhanced chemiluminescence system ECL-Plus, following the manufacturer's instructions, and exposed to X-ray film (Amersham Pharmacia Biotech, San Francisco, CA).

Quantification of NO and TNF-α released by BV2 microglia

Whole cell culture proteins were obtained in RIPA buffer (Santa Cruz Biotechnology, Santa Cruz, CA) as described previously (Ortega et al., 2012a).

The supernatant and the pellet were collected. NO production was assessed in culture supernatants by the Griess reaction, a colorimetric assay that detects nitrite (NO^{2-}) as a stable reaction product of NO with molecular oxygen (Virgili et al., 2011) . Briefly, 50 µL of each sample was incubated with 25 µL of Griess reagent A (1% sulfanilamide, 5% phosphoric acid) and 25 µL of Griess reagent B (0.1% N-1-naphthyl oenediamine) for 5 min. The optical density of the samples was measured at 540 nm using a microplate reader (Sunrise-Basic Reader, TECAN). The nitrite concentration was determined from a sodium nitrite standard curve. The amount of TNF-α released in the cell culture supernatants was determined using an ELISA murine TNF-α kit (PeproTech; London, UK) following the manufacturer's guidelines.

Statistical analysis

Kurtosis and Skewness moments were calculated to test the normal distribution of data. Variance homogeneity was checked by Cochran's C, Bartlett's, Hartley's, and Levene's tests. Association with continuous parameters was tested with one-way ANOVA followed by the Fisher's least significant difference (LSD) post-hoc test. Normality of residuals was checked by quantile-quantile plot analysis. When normality was not reached, the non-parametric Kruskal-Wallis (KW) test and then the Mann-Whitney U test were used to compare values for all groups All values are presented as mean ± standard error of the mean (SEM), and differences were considered to be significant at the $P<0.05$ level. Data were analyzed with the statistical analysis package StatGraphics 5.0 (STSC Inc., Rockville, MD, USA).

Results

Reactive microglia express $Ca_v1.2$ channels after NMDA-induced hippocampal lesion.

As described above, 20 nmol NMDA administration in the rat hippocampus induced a neurodegenerative process characterized at 15 days by a severe necrotic neuronal death and microglial reaction (Figure 1). Microscope observation of Nissl-stained sections revealed major NMDA-induced layer disorganization, neuronal loss and microgliosis in all layers of the hippocampal formation, including oriens, pyramidal, lacunosum-moleculare and radial strata of CA1, as well as in granular layers of the dentate gyrus (DG) (Figure 1A-B). This lesion covered an area of 3.2 ± 0.48 mm^2 (55% of the whole hippocampal formation area, Figure 1G). Counting of NeuN-immunopositive neurons indicated a mean 64% neuronal loss, affecting most hippocampal subfields and part of dentate gyrus (Fig. 1C-D). A maximum 79 ± 4% effect was reached in the CA1 pyramidal layer (Figure 1H), whose neuronal density (neurons/ mm^2), compared to the sham group, was reduced from 2154 ± 55 to 201 ± 6. In this hippocampal subfield, surviving neurons lost their characteristic pyramidal morphology and presented an abnormal shape of their soma and dendritic tree (detail in Figure 1C,D).

IB4 immunohistochemistry showed abundant microglia with reactive morphology, hypertrophy, hyperplasia and high IB4 immunostaining distributed over the entire lesioned area (Figure 1E-F), which evidenced a lesion-associated microgliosis. The area of this microgliosis reached 5.1 ± 0.97 mm^2 (87% of the whole hippocampal formation, Figure 1I). Morphology of IB4-labeled cells changed with their location and proximity to the injection site. The small cell body and several ramifications of resting microglia in healthy tissue

(detail in Figure 1E) changed progressively into a mixed reactive-amoeboid morphology in the core of the lesion (detail in Figure 1F). Counting of IB4-positive cells indicated a mean 46 ± 8% ($p = 0.03$) increase in the number of microglial cells in the lesioned hippocampus (not shown).

In control rats, immunohistochemistry with anti-rat α_{1C} antibody labeled the pyramidal CA1-CA3 cell layers of the hippocampus and the DG granular cell layer. Specific α_{1C}-immunoreactivity was also evident in the dendrites of the stratum radiatum and, less densely, in the stratum lacunosum-moleculare of CA1 (Figure 1J). The intense neuronal loss and layer disorganization induced by NMDA microinjection modified the distribution of hippocampal staining with a reduction in the pyramidal CA1 and granular DG layers which almost disappeared in the radiatum stratum of CA1 (Figure 1K). Surviving neurons that still expressed α_{1C} showed an abnormal morphology in pyramidal layers (Figure 1K1). However, non-neuronal specific anti-rat α_{1C} immunostaining (Figure 1K2) was observed homogeneously distributed in all lesioned hippocampal cell layers. Confocal microscopy and image analysis of double histochemistry with anti-α_{1C} antibody and IB4 revealed a clear expression of $Ca_v1.2$ channels in most amoeboid reactive microglia of the lesioned hippocampal formation (Figure 2D-F,K). Image analysis revealed specific anti-α_{1C} antibody labelling located at the cytoplasma and the plasma membrane of 36 ± 8% IB4 positive cells (Figure 2D-F) The mean values of co-localization parameters from MDP images were: Pearson's r = 0.430, overlap coefficients R = 0,589, k1 = 0.712, and k2 0.675 (n = 6 different MDP images from 3 lesioned rats) (Figure 2G-I). Specific anti-α_{1C} staining did not co-localize IB4 stainig in some reactive cells of the lesioned hippocampus. Co-localization of anti-α_{1C} antibody and IB4 staining

was not found in the hipocampus of control rats (Pearson's r = 0.065, R = 0.462, k1 = 0.699, and k2 = 0.304; n = 6 different MDP images from 3 control rats). (Figure 2A-C, J).

BV2 microglia express α_1 subunits of L-type VGCC

To study the functions of the L-type VGCC in microglial cells *in vitro*, we first analyzed the expression of $Ca_v1.2$ and $Ca_v1.3$ channels by RT-PCR analysis of total RNA extracted from three different cultures of the activated murine microglia-derived cell line BV2. We examined the expression of the L-type VGCC by analyzing distinct pore-forming α_1 subunit PCR products. The PCR products for α_{1C} ($Ca_v1.2$) and α_{1D} ($Ca_v1.3$) found in the RNA preparation of BV2 were comparable to those obtained from whole brain RNA preparations used as positive controls (Figure 3A-B).

The presence of α_{1C} protein in microglial BV2 was studied by Western blotting of the membrane protein extracts isolated from three different cultures of BV2 cells. A positive signal was observed at 240 KDa (Figure 3C), indicating the presence of the L-type VGCC in the microglial membrane. Compared to quiescent cells, densitometry quantification evidenced a significant 63 ± 7% increase (n= 5 different cultures; p=0.0072) in the expression of α_{1C} protein in BV2 cells activated with LPS and IFNγ during 24 hours. Immunofluorescence localized α_{1C} in BV2 cells and complemented western blotting and PCR results (Figure 3D-F). Specific α_{1C} immunoreactivity was clearly located at the plasma membrane and characteristic membrane processes of BV2 cells stimulated with LPS+IFNγ (Figure 3F), whereas non-activated BV2 cells presented a weak immunostaining similar to background (Figure 3E).

L-type VGCC specific drugs modify KCl-induced intracellular calcium increase in BV2 microglia

Application of high K^+ concentrations in the culture medium has classically been used to depolarize the cell membrane and consequently to activate voltage-operated channels. To study whether cell membrane depolarization is able to produce an $[Ca^{2+}]_i$ increase in activated microglia, control and LPS+IFNγ stimulated BV2 cells were loaded with the fluorescent intracellular calcium probe Fura-2 and monitored. We used 10 μM Nifedipine as specific L-type VGCC blocker and 10 μM Bay k8644 as specific openner of the channel (Figure 4A-B).

In control cells, the basal F_{340}/F_{380} ratio was 0.223 ± 0.008 and no spontaneous intracellular calcium oscillations were observed in these conditions. Addition of 10 μm nifedipine or 10 μm Bay k8644 did not modify this ratio (F_{340}/F_{380} values were 0.203 ± 0.01 and 0.236 ± 0.02 respectively; KW = 7.671, p = 0.175) and no spontaneous intracellular calcium oscillations were observed in these conditions. Addition of 80 mM KCl to the medium increased $[Ca^{2+}]_i$ to a F_{340}/F_{380} ratio of 0.2987 ± 0.03 in 42% of control BV2 cells (45 out of 107, from 3 different assays) (Figure 4C-D). In these responding cells, the mean amplitude of the response increased a 28.2 % the F_{340}/F_{380} ratio from the baseline level (Figure 4E), with a mean duration of 180 seconds. Trypan blue staining showed that the cell viability was not compromised by the calcium response to high potassium levels. 10 μM nifedipine decreased the F_{340}/F_{380} ratio to a mean value of 0.2198 ± 0.01 and the number of control BV2 cell responding to KCl to 35.9%. Bay k8644 did not modified the ratio but increased the percent number of responding cells until 52.5% (KW = 9.955, p=0.0016) (Figure 4C, D). Both drugs

also modified the mean amplitude of $[Ca^{2+}]_i$ increase in responding cells. In presence of nimodipine the KCl-induced F_{340}/F_{380} ratio increased 23% from the baseline level, whereas in the presence of Bay k8644 the ratio increased 37% from the baseline level (KW = 8.557, p=0.0136) (Figure 4E).

In cells stimulated with LPS+IFNγ the basal F_{340}/F_{380} ratio was 0.221 ± 0.03. Addition of 10 μm nifedipine or 10 μm Bay k8644 did not modified this ratio (mean values 0.2163 ± 0.03 and 0.2461 ± 0.04 respectively, KW = 6.521, p = 0.535). 81% of LPS+IFNγ stimulated cells (165 out of 204, from 7 different assays) showed an increase of $[Ca^{2+}]_i$ to a ratio of 0.307 ± 0.03 due to 80 mM KCl (Figure 4C-D). In these responding cells, the mean amplitude of the response increased the ratio a 27.8 % from the baseline level (Figure 4E), with a mean duration of 180 seconds. When 10 μM nifedipine was added to 80 mM KCl, the response of LPS+IFNγ-stimulated cells fell significantly (Figure 4C-D). Only 42% of cells responded (109 out of 261 from 7 different assays), the mean F_{340}/F_{380} ratio decreased to 0.2503 ± 0.03 (Figure 4C) ($F_{3,250}$ = 90.07, p = 0.00001), which correnponded to a 27.8 % increase from the baseline level in responding cells (Figure 4E). Nifedipine also changed the time to reach the maximal calcium concentration (T_{peack}) of the response from 31.4 ± 3.34 s to 63.1 ± 2.29 s (p< p.05), whereas the duration of the intracellular calcium increase remained practically unaltered (Figure 4A).

Addition of 10 μM Bay k8644 to the medium increased significantly the response of activted BV2 cells to 80 mM KCl (Figure 4C-E). In the presence of Bay k8644, 78.8% of cells showed a higher increase of $[Ca^{2+}]_i$ due to KCl with a F_{340}/F_{380} ratio of 0.351 ± 0.04, which corresponded to a 31.3% increase from the base line (64 out of 81 cells from 3 different experiments; KW = 4.459, p =

0.032). Bay k8644 incubation also sligthly increased the T_{peack} of the response 63.1 ± 2.29 s (p< p.05), slightly increased the (Figure 4B).

L-type VGCC blockade decreases the pro-inflammatory response but does not modify the phagocytic capacity of BV2 microglia

To investigate the role of the L-type VGCC in the control of microglial pro-inflammatory signal release, 24 hours after activation with LPS+IFNγ BV2 cells were incubated with either 10 µM nifedipine, 25 µM nimodipine, or 10 µM Bay k8644, and NO production and TNF-α concentration were determined 24 hours later (Figure 5). Compared with control BV2 microglia, incubation with LPS+IFNγ increased NO (6-fold) and TNF-α (5-fold) production. Treatment of non-activated microglia with either nimodipine, nifedipine or bay k8644 did not significantly modified the extracellular concentrations of nitrite and TNF- α (Figure 5A-F). Treatment of activated BV2 microglia with 10 µM nifedipine during 24 hours significantly decreased the extracellular concentrations of nitrite (40% decrease, $F_{2,12}$ = 13.39, p = 0.0009) and TNF-α (44% decrease, $F_{2,6}$ = 7.11, p = 0.0261) (Figure 5A,B). Incubation with 25 µM nimodipine gave similar results with a drastic 75% decrease of nitrite production ($F_{2,12}$ = 9.511, p = 0.039) and a 51% decrease in TNF-α ($F_{2,12}$ = 14.27, p = 0.0003) (Figure 5C,D). 10 µM Bay k8644 did not significantly modified the extracellular concentrations of nitrite and TNF-α (Figure 5E,F).

Although the same stimulus can trigger microglial secretion of inflammatory signals and activation of phagocytosis, it has been proposed that they are regulated by different intracellular pathways (Kettenmann et al., 2011). In view of this we also investigated the role of the L-type VGCC in the control of phagocytic capacity of BV2 microglia (Figure 6A-I). The analysis was performed

48 hours after activation with LPS+IFNγ and 30 min after fluorosphere incubation. Activation of BV2 microglia with LPS+IFNγ increased the percentage of cells presenting FluoroSpheres in the cytoplasm ($F_{2,33}$ = 402.19, p = 0.00001) as well as the number of FluoroSpheres within the cells ($F_{2,33}$ = 7.41, p = 0.0022). Treatment with 10 µM nifedipine had no effect on this phagocytic capacity (Figure 6J-K).

Discussion

Here we demonstrate the expression of α_1 subunits of L-Type VGCC in reactive microglia during excitotoxicity in the rat hippocampus and in cultured BV2 cells, in which nifedipine blocks the K^+-induced $[Ca^{2+}]_i$ elevation and inhibits the pro-inflammatory activity of reactive microglia, and Bay k8644 enhances $[Ca^{2+}]_i$ elevation. Evidence for microglial VGCC currents is limited to a single report, in which voltage-clamp experiments revealed a small inward Ca^{2+} current in 30% of the cells tested (Colton et al., 1994). Additional indirect evidence showed that treatment of cultured rat microglial cells with high K^+ solutions enhanced superoxide anion production induced by phorbol 12-myristate 13-acetate, an effect that was blocked by nifedipine (Colton et al., 1994). These pharmacological observations are consistent with our *in vivo* and *in vitro* results, which provide direct molecular evidence of functional L-type VGCC expression by reactive BV2 microglia. Thus, the L-type VGCC emerges as a new player in the calcium-mediated signaling in microglia.

The elevation of baseline $[Ca^{2+}]_i$ is a central element in the regulation of certain executive functions in activated microglia (Kettenmann et al., 2011). *In vitro* microglial activation with LPS leads to a chronic elevation of $[Ca^{2+}]_i$ in microglial

cells and a suppression of evoked calcium signaling (Hoffmann et al., 2003). Lowering the intracellular calcium with BAPTA restored much of the signaling efficacy. BAPTA also strongly attenuated the LPS-induced release of NO, TNF-α, IL-6, IL-12, and other chemokines (Färber and Kettenmann, 2006). Furthermore, when isolated from Alzheimer's brain patients in the vicinity of amyloid plaques and compared with controls, reactive microglia had a higher resting calcium level and reduced response amplitude to ATP (McLarnon, 2005). Some evidence indicates that L-type VGCC may account for some of these $[Ca^{2+}]_i$ changes. For instance, amyloid-beta peptides are able to induce *in vitro* microglial activation and elicit an increase in $[Ca^{2+}]_i$ levels which are abolished by specific L-type VGCC blockers such as verapamil, nifedipine and diltiazem (Silei et al., 1999). Moreover, other calcium entry pathways are likely to be important in the regulation of microglial activity. For instance, a role for N-type VGCC has been proposed in the pathogenesis of experimental autoimmune encephalomyelitis by regulating the microglial production of the monocyte chemoattractant protein-1 (Tokuhara et al., 2010).

Microglia respond to damage by up-regulating functions that involve calcium signaling, such as proliferation, migration, phagocytosis and production of pro-inflammatory cytokines, chemokines and trophic factors (Färber and Kettenmann, 2006). The up-regulation of the L-type VGCC in microglia may, therefore, have different pathophysiological implications. The effects of nifedipine and nimodipine on the secretion of NO and TNF-α by BV2 microglia evidence a role of this channel in microglial synthesis and the release of pro-inflammatory substances. The discrete effects of Bay k8644 on the secretion of

NO and TNF-α by non-stimulated microglia suggest the L-type VGCC is not sufficient to induce such release and it has a modulatory role.

The anti-inflammatory effect of L-type VGCC blockade appears to be specific, since phagocytosis could not be modulated by nifedipine. In mixed cultures, L-type VGCC blockers such as nimodipine inhibit NO production and TNF-α, IL-1β and prostaglandin E2 secretion from LPS-stimulated microglia accompanied and reduced the degeneration of dopaminergic neurons (Li et al., 2009). However, other functional implications of the L-type VGCC should not be ruled out. For example, the expression of this channel may not be a consequence of cell activation but an essential step in the phenotypic transition into the activated microglia state. Also, certain results suggest a role for the L-type VGCC in the control of proliferation and migration of activated microglia. For example, CCL5, a β-chemokine involved in immune responses including migration (Maghazachi, 2000), secretion (Logan et al., 2003) , and gene expression (Crabtree and Olson, 2002), specifically activates a nimodipine-sensitive calcium current in microglia (Shideman et al., 2006).

The vulnerability of the CNS to excitotoxic insults and hypoxia-ischemia differs according to brain areas (Rodríguez et al., 2009b). The microglial expression of the L-type VGCC described here may contribute to explaining this differential vulnerability. In pathological processes, microglia show a hybrid activation state that includes inflammatory actions and also characteristics of neuroprotection and repair (Graeber and Streit, 2010). Whether microglia adopt a phenotype that mostly exacerbates tissue injury or promotes brain repair probably depends on the diversity of signals from the lesion environment. Similarly, the expression level of calcium channels in microglia seems to be regulated by

microenvironmental factors and depends on the functional state of the cell (Kettenmann et al., 2011). Consequently, the expression of the L-type VGCC in activated microglia may be central in determining, at least in part, their participation in the pathogenic process. Inside this framework, dihydropyridine drugs such as nifedipine and nimodipine have neuroprotective properties (Schurr, 2004), although until now this property has not been ascribed to anti-inflammatory effects. Thus, examining the potential immunomodulatory properties of these drugs might help to clarify the controversial effectiveness of calcium channel antagonists in experimental and clinical assays.

Conclusion

To sum up, our results provide clear evidence of the expression of α_1 subunits of the L-type VGCC in reactive microglia during excitotoxicity in the rat hippocampus and in cultured BV2 cells. We also provide evidence of a role of the L-type VGCC in the control of the pro-inflammatory activity of reactive microglia. Taken together, these results suggest a leading role for the L-type VGCC in the control of microglial secretory activity during inflammatory processes of the CNS. Further experiments are needed to clarify the specific molecular mechanisms activated by this channel and its role on the prevention of neuronal cell loss induced by proinflammatory microglial activity. Their characterization would help to ascertain other putative functional implications of the L-type VGCC in the control of microglial functions.

List of abbreviations used

$[Ca^{2+}]i$: Intracellular calcium concentration; DAB: Diaminobenzidine; DG: Dentate gyrus; FBS: Fetal bovine serum; GFAP: Glial fibrillary acidic protein;

IB4: Isolectin B4; IFNγ: Interferon-gamma; IL-1β: Interleukin-1β; KW: Kruskal-Wallis; LPS: Lipopolysaccharide; LSD: Least significant difference; MDP: Mean deviation product; NGS: Normal goat serum; NMDA: N-methyl-D-aspartate; PBS: Phosphate buffer saline; SEM: Standard error of the mean; TNF-α: Tumor necrosis factor alpha.

Competing interests

The authors declare that they have no conflict of interest.

Author's contributions

NM & MJR got financial support for the study. JFE-P & MJR designed the study. MM-M, JFE-P & XG performed the experiments. JFE-P, MM-M, XG, NM & MJR analyzed and discussed the results. MM-M, NM & MJR wrote the manuscript

Acknowledgements

This research was supported by grants IPT- 2011-1091-900000 and IPT-2012-0614-010000 from the Ministerio de Economia, and by grant 2014SGR1115 from the Generalitat de Catalunya, Spain.

References

Ashcroft FM, Proks P, Smith PA, Ammälä C, Bokvist K, Rorsman P. 1994. Stimulus-secretion coupling in pancreatic beta cells. J Cell Biochem 55 Suppl:54–65.

Bading H, Ginty DD, Greenberg ME. 1993. Regulation of gene expression in hippocampal neurons by distinct calcium signaling pathways. Science 260:181–186.

Bataller R, Gasull X, Ginès P, Hellemans K, Görbig MN, Nicolás JM, Sancho-Bru P, De Las Heras D, Gual A, Geerts A, Arroyo V, Rodés J. 2001. In vitro and in vivo activation of rat hepatic stellate cells results in de novo expression of L-type voltage-operated calcium channels. Hepatology 33:956–962.

Bean BP. 1989. Neurotransmitter inhibition of neuronal calcium currents by changes in channel voltage dependence. Nature 340:153–156.

Berg M, Bruhn T, Frandsen A, Schousboe A, Diemer NH. 1995. Kainic acid-induced seizures and brain damage in the rat: role of calcium homeostasis. J. Neurosci Res 40:641–646.

Bernal F, Petegnief V, Rodríguez MJ, Ursu G, Pugliese M, Mahy N. 2009. Nimodipine inhibits TMB-8 potentiation of AMPA-induced hippocampal neurodegeneration. J Neurosci Res 87:1240–1249.

Catterall WA, Perez-Reyes E, Snutch TP, Striessnig J. 2005. International Union of Pharmacology. XLVIII. Nomenclature and structure-function relationships of voltage-gated calcium channels. Pharmacol Rev 57:411–425.

Colton CA, Jia M, Li MX, Gilbert DL.1994. K^+ modulation of microglial superoxide production: involvement of voltage-gated Ca^{2+} channels. Am J Physiol 266:C1650–1655.

Colton CA, Wilcock DM. 2010. Assessing activation states in microglia. CNS Neurol Disord Drug Targets 9:174–191.

Crabtree GR, Olson EN. 2002. NFAT signaling: choreographing the social lives of cells. Cell 109 Suppl:S67–79.

Damani MR, Zhao L, Fontainhas AM, Amaral J, Fariss RN, Wong WT. 2011. Age-related alterations in the dynamic behavior of microglia. Aging Cell 10:263–276.

Domercq M, Vázquez-Villoldo N, Matute C. 2013. Neurotransmitter signaling in the pathophysiology of microglia. Front Cell Neurosci 7:49.

Färber K, Kettenmann H. 2006. Purinergic signaling and microglia. Pflugers Arch 452:615–621.

Frandsen A, Schousboe A, Griffiths R. 1993. Cytotoxic actions and effects on intracellular Ca^{2+} and cGMP concentrations of sulphur-containing excitatory amino acids in cultured cerebral cortical neurons. J Neurosci Res 34:331–339.

Fryer HJ, Knox RJ, Strittmatter SM, Kalb RG. 1999. Excitotoxic death of a subset of embryonic rat motor neurons in vitro. J Neurochem 72:500–513.

Graeber MB, Streit WJ. 2010. Microglia: biology and pathology. Acta Neuropathol 119:89–105.

Hegg CC, Hu S, Peterson PK, Thayer SA. 2000. Beta-chemokines and human immunodeficiency virus type-1 proteins evoke intracellular calcium increases in human microglia. Neuroscience 98:191–199.

Hoffmann A, Kann O, Ohlemeyer C, Hanisch U-K, Kettenmann H. 2003. Elevation of basal intracellular calcium as a central element in the activation

of brain macrophages (microglia): suppression of receptor-evoked calcium signaling and control of release function. J Neurosci 23:4410–4419.

Horn J, de Haan RJ, Vermeulen M, Limburg M. 2001. Very Early Nimodipine Use in Stroke (VENUS): a randomized, double-blind, placebo-controlled trial. Stroke 32:461–465.

Jaskolski F, Mulle C, Manzoni OJ. 2005. An automated method to quantify and visualize colocalized fluorescent signals. J Neurosci Methods 146:42–49.

Kettenmann H, Hanisch U-K, Noda M, Verkhratsky A. 2011. Physiology of microglia. Physiol Rev 91:461–553.

Li Y, Hu X, Liu Y, Bao Y, An L. 2009. Nimodipine protects dopaminergic neurons against inflammation-mediated degeneration through inhibition of microglial activation. Neuropharmacology 56:580–589.

Liao B, Zhao W, Beers DR, Henkel JS, Appel SH. 2012. Transformation from a neuroprotective to a neurotoxic microglial phenotype in a mouse model of ALS. Exp Neurol 237:147–152.

Lipscombe D, Helton TD, Xu W. 2004. L-type calcium channels: the low down. J Neurophysiol 92:2633–2641.

Logan MR, Odemuyiwa SO, Moqbel R. 2003. Understanding exocytosis in immune and inflammatory cells: the molecular basis of mediator secretion. J. Allergy Clin Immunol 111:923–932; quiz 933.

Maghazachi AA. 2000. Intracellular signaling events at the leading edge of migrating cells. Int J Biochem Cell Biol 32:931–943.

Manders EMM, Verbeek FJ, Aten JA. 1993. Measurement of co-localisation of objects in dual-colour confocal images. J Microscopy 169:375–382.

Mattsson P, Aldskogius H, Svensson M. 1999. Nimodipine-induced improved survival rate of facial motor neurons following intracranial transection of the facial nerve in the adult rat. J Neurosurg 90:760–765.

McLarnon JG. 2005. Purinergic mediated changes in Ca^{2+} mobilization and functional responses in microglia: effects of low levels of ATP. J Neurosci Res 81:349–356.

Ortega FJ, Gimeno-Bayon J, Espinosa-Parrilla JF, Carrasco JL, Batlle M, Pugliese M, Mahy N, Rodríguez MJ. 2012a. ATP-dependent potassium channel blockade strengthens microglial neuroprotection after hypoxia-ischemia in rats. Exp Neurol 235:282–296.

Ortega FJ, Vidal-Taboada JM, Mahy N, and Rodríguez MJ. 2012b. Molecular mechanisms of acute brain injury and ensuing neurodegeneration. In A. González-Quevedo ed. Brain Damage - Bridging between basic research and clinics. Rijeka InTech, pp. 163-186.

Ortega FJ, Jolkkonen J, Mahy N, Rodríguez MJ. 2013. Glibenclamide enhances neurogenesis and improves long-term functional recovery after transient focal cerebral ischemia. J Cereb Blood Flow Metab 33: 356-364.

Paxinos G and Watson J. 1986. The rat brain in stereotaxic coordinates. Academic Press.

Petegnief V, Ursu G, Bernal F, Mahy N. 2004. Nimodipine and TMB-8 potentiate the AMPA-induced lesion in the basal ganglia. Neurochem Int 44:287–291.

Rami A, Krieglstein J. 1994. Neuronal protective effects of calcium antagonists in cerebral ischemia. Life Sci 55:2105–2113.

Rodríguez MJ, Ursu G, Bernal F, Cusí V, Mahy N. 2001. Perinatal human hypoxia-ischemia vulnerability correlates with brain calcification. Neurobiol. Dis 8:59–68.

Rodríguez MJ, Prats A, Malpesa Y, Andrés N, Pugliese M, Batlle M, Mahy N. 2009a. Pattern of injury with a graded excitotoxic insult and ensuing chronic medial septal damage in the rat brain. J Neurotrauma 26:1823–1834.

Rodríguez MJ, Pugliese M, and Mahy N. 2009b. Drug abuse, brain calcification and glutamate-induced neurodegeneration. Curr Drug Abuse Rev 2:99-112.

Rodríguez MJ, Martinez-Moreno M, Ortega FJ, Mahy N. 2013. Targeting microglial K_{ATP} channels to treat neurodegenerative diseases: a mitochondrial issue. Oxid Med Cell Long 2013:194546.

Schurr A. 2004. Neuroprotection against ischemic/hypoxic brain damage: blockers of ionotropic glutamate receptor and voltage sensitive calcium channels. Curr Drug Targets 5:603–618.

Shideman CR, Hu S, Peterson PK, Thayer SA. 2006. CCL5 evokes calcium signals in microglia through a kinase-, phosphoinositide-, and nucleotide-dependent mechanism. J Neurosci Res 83:1471–1484.

Silei V, Fabrizi C, Venturini G, Salmona M, Bugiani O, Tagliavini F, Lauro GM. 1999. Activation of microglial cells by PrP and beta-amyloid fragments raises intracellular calcium through L-type voltage sensitive calcium channels. Brain Res 818:168–170.

Small DL, Monette R, Buchan AM, Morley P. 1997. Identification of calcium channels involved in neuronal injury in rat hippocampal slices subjected to oxygen and glucose deprivation. Brain Res. 753:209–218.

Soto D, Comes N, Ferrer E, Morales M, Escalada A, Palés J, Solsona C, Gual A, Gasull X. 2004. Modulation of aqueous humor outflow by ionic mechanisms involved in trabecular meshwork cell volume regulation. Invest Ophthalmol Vis Sci 45:3650–3661.

Strober W. 2001. Trypan blue exclusion test of cell viability. Curr Protoc

Immunol Appendix 3:Appendix 3B.

Toba Y, Pakiam JG, Wray S. 2005. Voltage-gated calcium channels in developing GnRH-1 neuronal system in the mouse. Eur J Neurosci 22:79–92.

Tokuhara N, Namiki K, Uesugi M, Miyamoto C, Ohgoh M, Ido K, Yoshinaga T, Yamauchi T, Kuromitsu J, Kimura S, Miyamoto N, Kasuya Y. 2010. N-type calcium channel in the pathogenesis of experimental autoimmune encephalomyelitis. J Biol Chem 285:33294–33306.

Virgili N, Espinosa-Parrilla JF, Mancera P, Pastén-Zamorano A, Gimeno-Bayon J, Rodríguez MJ, Mahy N, Pugliese M. 2011. Oral administration of the K_{ATP} channel opener diazoxide ameliorates disease progression in a murine model of multiple sclerosis. J Neuroinflamm 8:149.

Virgili N, Mancera P, Chanvillard C, Wegner A, Wappenhans B, Rodríguez MJ, Infante-Duarte C, Espinosa-Parrilla JF, Pugliese M. 2014. Diazoxide attenuates autoimmune encephalomyelitis and modulates lymphocyte proliferation and dendritic cell functionality. J Neuroimm Pharmacol 9:558–568.

Zamponi GW, Snutch TP. 2013. Advances in voltage-gated calcium channel structure, function and physiology. Biochim Biophys Acta 1828:1521.

Zhang H, Wang FW, Yao LL, Hao AJ. 2011. Microglia--friend or foe. Front Biosci. (Schol Ed) 3:869–883.

Zhu D, Li R, Liu G, Hua W. 1999. Nimodipine inhibits calcium-independent nitric oxide synthase activity in transient focal cerebral ischemia rats and cultured mouse astroglial cells. Life Sci 65:PL221–231.

FIGURE LEGENDS

Figure 1. Effects of NMDA injection and immunodetection of α_{1C} subunit in the rat hippocampus. Illustrative microphotographs of cresyl-violet stained hippocampal sections of sham (A) and NMDA lesioned rats (B) showing the hippocampal layer disorganization, neuronal loss, and glial reaction 15 days after NMDA injection. NeuN immunostaining of the hippocampus of sham (C) and NMDA rats (D) shows the neuronal loss as an area of devoid of immunoreactivity. Insets in C-D illustrate the morphology of stained pyramidal neurons inside the square in sham and NMDA lesioned rats. IB4 staining of the hippocampus of sham (E) and NMDA rats (F) as an estimation of the microglial reaction to NMDA injection. Insets in E-F illustrate the morphology of stained cells inside the square in sham and NMDA lesioned rats. Graphs show the quantification of: (G) the area of lesion measured on Nissl stained sections, (H) the percent of neuronal loss in the pyramidal stratum of *Cornu Ammonis* 1 measured in NeuN-immunostaimed sections and (I) thearea of microglia reaction measured on IB4 stained hippocampal sections. (J) Specific neuronal α_{1C}-immunoreactivity was observed in sham rats, with clear staining in neuronal processes of the pyramidal (J1) and radiatum (J2) strata of *Cornu Ammonis* 1. (K) NMDA induced disorganization of pyramidal stratum of Cornu Ammonis 1 was evidenced by α_{1C} immunostaining (K1). A non-neuronal specific anti-rat α_{1C} immunostaining was also observed in NMDA-lesioned hippocampus, which was evident in the radiatum (K2) stratum of *Cornu Ammonis* 1. PyrCA1, pyramidal stratum of *Cornu Ammonis;* DG, dentate gyrus. Arrows in A-F indicate the injection site. Scale bar 1 mm; insets, K1 and K2, 50 μm.

Figure 2. Expression of α_{1C} in activated IB4-positive cells in the hippocampus of NMDA ,Klesioned rats. (A-C, J) Stack images of double immunohistochemistry of α_{1C} (green) and IB4 (red) in the hippocampus of sham animals. (D-F, K) Stack images of double immunohistochemistry of α_{1C} and IB4 in the hippocampus of NMDA-lesioned rats with some IB4-positive cells also positive for α_{1C} (white arrows). Confocal analysis of the image of a XY plane (G) with the merged channels, the MDP map of the image (H), and the scatter plot (I). The presence of yellow dots in G, H and I denotes the presence of IB4 and α_{1C} colocalization for both channels, in which IB4-postive cells of the lesioned hippocampus express α_{1C}. Colocalization parameters from (I) are Pearson's r = 0.413, Overlap coefficient = 0.685, Overlap coeficient for green (k1) = 0.739 and for red (k2) = 0.635. Scale bar 40 μm for A-F; 100 μm for G-H, 10 μm for J, K.

Figure 3. Expression of the L-type VGCC in BV2 microglia. Murine BV2 cell culture was analyzed 48h after activation with LPS+IFNγ (see material and methods for details). RT-PCR analyses of L-Type VGCC subunits were performed with gene-specific primers. PCR products for α_{1D} (A) and (B) α_{1C} subunits (arrows) were separated by 1.5% agarose gel electrophoresis and stained with ethidium bromide. Each gel was loaded with standard size markers (line 1) and cDNA amplified from brain as control (brain); c, non-activated BV2 cells; L+I, BV2 cells activated with LPS+IFNγ; Hek, total RNA from HEK293 cells (used as negative PCR control). Amplified fragments had the sizes of 226 bp for α_{1D} and 223 bp for α_{1C}, as predicted by the mRNA sequence amplicons (n= 3 different cultures). (C) Immunoblot and densitometry quantification of α_{1C} expressed by control (c) and activated (L+I) BV2 cells. Homogenates were normalized for protein content quantified by Bradford's method, 15 mg of protein

was applied in each gel lane and each sample was loaded into two lanes. Bands appeared at the level of 240 kDa; for quantification, β-Actin immunoblott was used as loading control (n= 5 different cultures) (D-F): Immunocytochemistry with specific antibodies against α_{1C} was performed in control (E) and BV2 cells activated with LPS+IFNγ (F) Specificty of the antibody was assessed in control cells by immunodetection in absence of primary antibody (D). Specific binding (arrowheads in F) was detected with AlexaFluor 488-conjugated secondary antibodies (green). Note that activated BV2 cells are larger and showed numerous processes, as published elsewhere (Ortega et al., 2012a; see also Figure 5). (n= 3 different cultures). Scale Bar 20 μm.

Figure 4. Effects of pharmacological modulation of the L-type VGCC on intracellular calcium permeability of BV2 microglia. (A-B) Illustrative representation of $[Ca^{2+}]_i$ kinetics in one single activated BV-2 cell before and after 2 min depolarization with 80 mM KCl (black bar). (A) Addition in the bath of 10 μM nifedipine for 3 min (Nif, gray bar) significantly reduced the increase of $[Ca^{2+}]_i$ induced by KCl (dashed line vs continuous line). (B) Addition in the bath of 10 μM Bayk for 3 min (gray bar) significantly enhanced the increase of $[Ca^{2+}]_i$ induced by KCl. (dashed line vs continuous line) (C) Histogram showing the 340- to 380-nm fluorescence ratios as an estimation of the $[Ca^{2+}]_i$ changes induced by 80 mM KCl addition in control and LPS+IFNγ activated BV2 cells (L+I) loaded with Fura-2. Effects of L-type VGCC on $[Ca^{2+}]_i$ changes were assessed by addition of either 10 μM Nifedipine (Nif) or 10 μM Bay k8644 (Bayk). n = 154 cells in control (70 for KCl, 46 for KCl+Nif –both from 7 different experiments- and 38 for KCl+Bayk -from 3 different experiments-) and n = 280 cells in L+I (151 cells for KCl, 83 cells for KCl+Nif –both from 7 different

cultures- and 46 cells for KCl+Bayk –from 3 different cultures-) (D) Histogram shows the percent of cells responding to 80 mM KCl in control and L+I activated cells in all six conditions. (E) Histogram shows the percent of $[Ca^{2+}]_i$ changes induced by 80 mM KCl found in the responsive cells in the six conditions studied. * p<0,05 compared with KCl control, # p < 0.05 compared with KCl L+I (Mann-Whitney test). Values are presented as mean ±SEM

Figure 5. Effects of pharmacological modulation of the L-type VGCC on the pro-inflammatory response of BV2 microglia. Histograms show TNF-α release and NO production of control and LPS+IFNγ activated (L+I) BV2 cells assessed 48h after activation, and post-treated with either (A,B) 10 µM nifedipine (Nif, n = 7 different cultures), (C,D) 25 µM nimodipine (Nim, n = 3 different cultures) or (E,F) 10 µM Bay k8644 (BayK, n = 3 different cultures) for 24 hours. NO production was quantified by the Griess method and TNF-α release was quantified by ELISA * p<0,05 compared with control, # p < 0.05 compared with L+I (Mann-Whitney test). Values are presented as mean ± SEM

Figure 6. Nifedipine does not modify the phagocytic activity of reactive BV2 microglia. The phagocytic capacity of BV2 cells was assessed 48h after activation with LPS+IFNγ and post-treated with 10 µM Nifedipine, (A-J) Illustrative microphotographs of the effects of nifedipine on the phagocytosis of FluoroSpheres (red) by BV2 microglia (green). Graphs show the quantification of the BV2-cell phagocytic capacity measured using the FluoroSpheres assay (see material and method for details). The estimated phagocytic parameters were the number of spheres per cell (K) and the percentage of phagocytic cells (L). (n = 4 cultures, * p < 0.05 compared with Control, LSD posthoc). Scale bar: 10 µm.

Figure 1: Effects of NMDA injection and immunodetection of α_{1C} subunit in the rat hippocampus

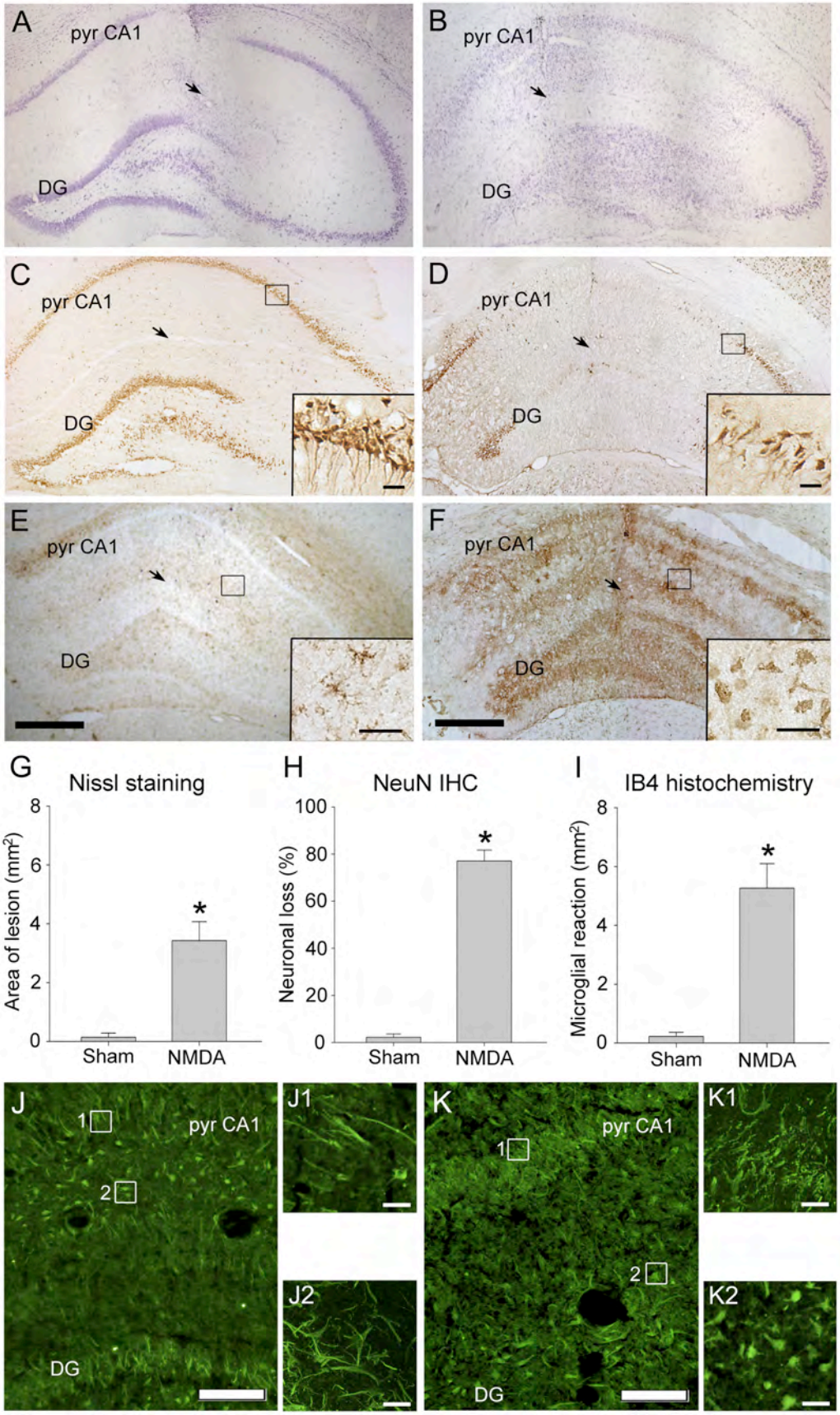

Figure 2: Expression of α_{1C} in activated IB4-positive cells in the hippocampus of NMDA-lesioned rats.

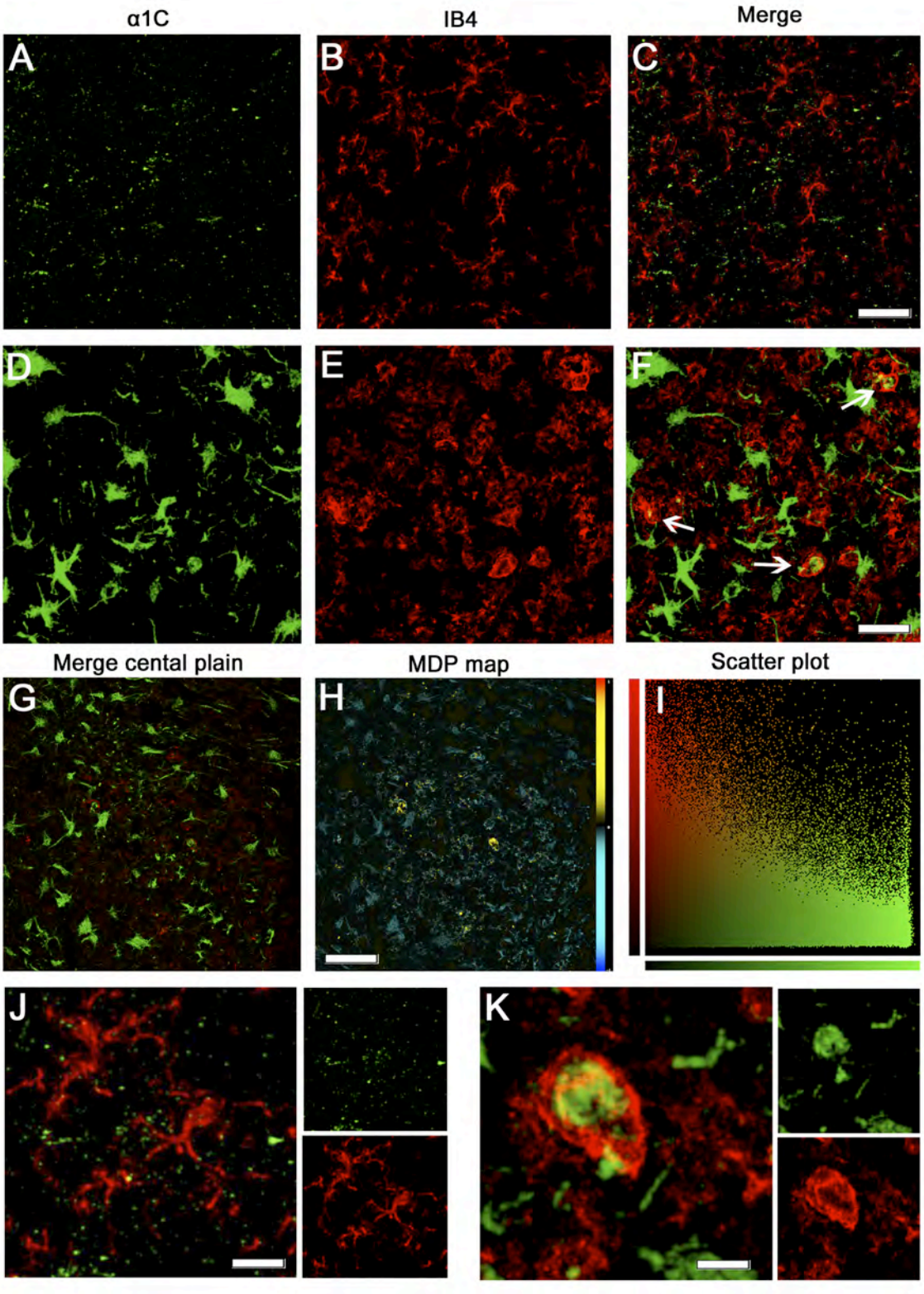

Figure 3: Expression of the L-type VGCC in BV2 microglia.

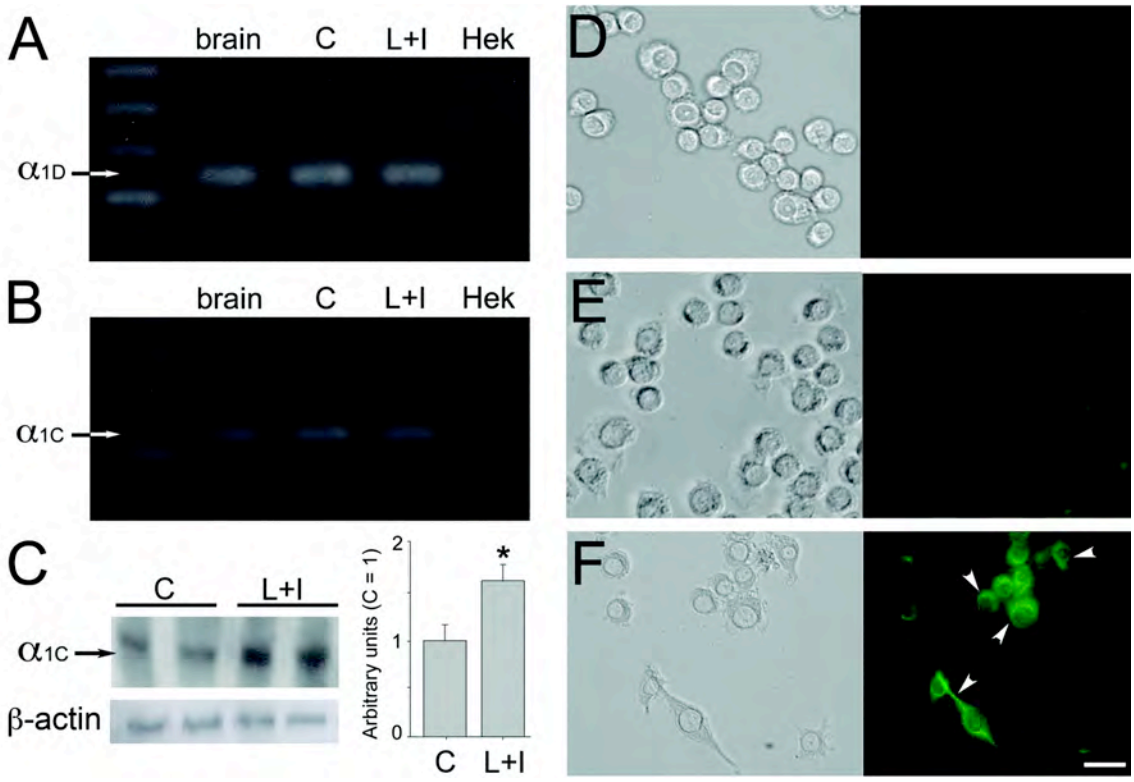

Figure 4: Effects of pharmacological modulation of the L-type VGCC on intracellular calcium permeability of BV2 microglia.

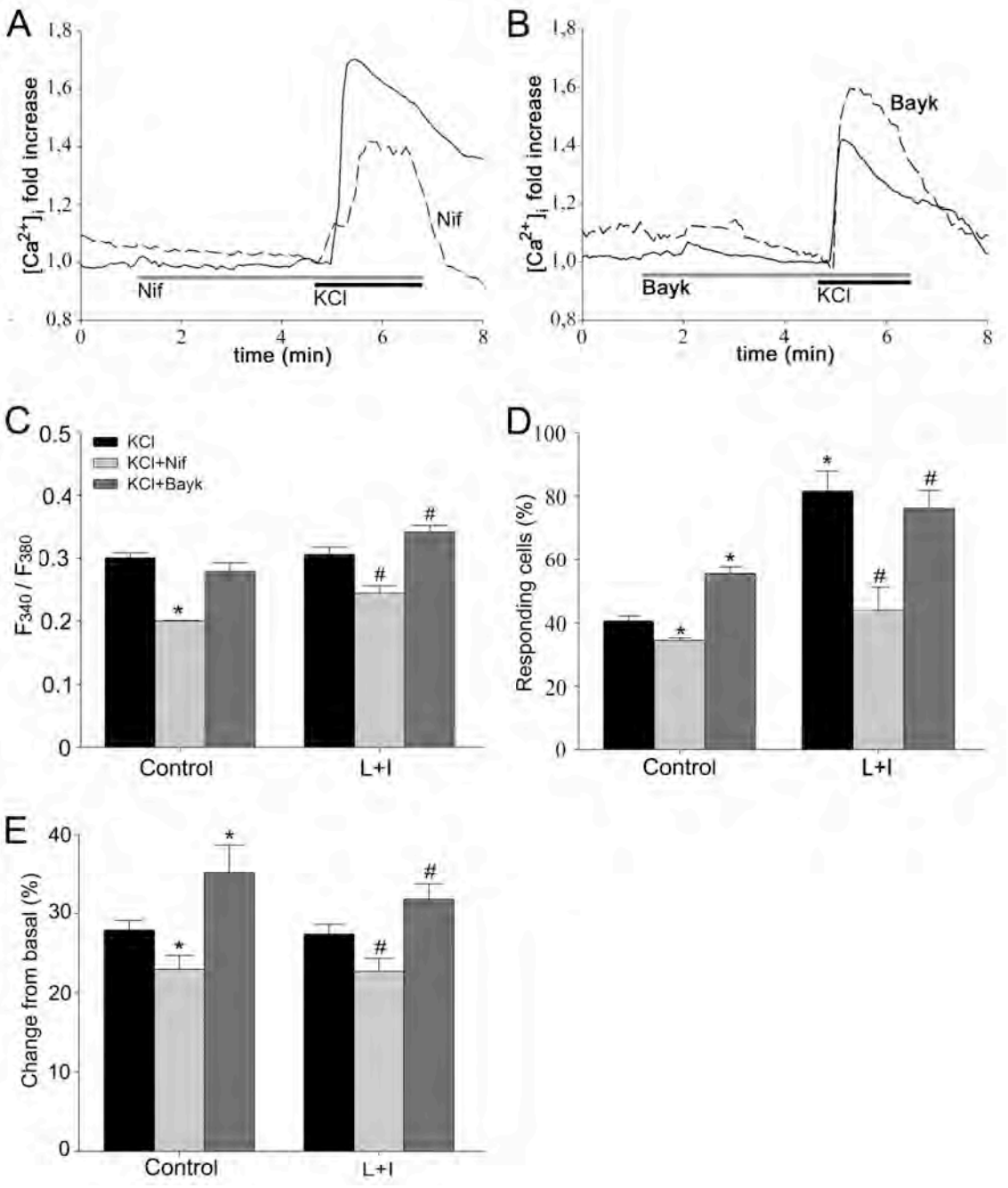

Figure 5: Effects of pharmacological modulation of the L-type VGCC on the pro-inflammatory response of BV2 microglia.

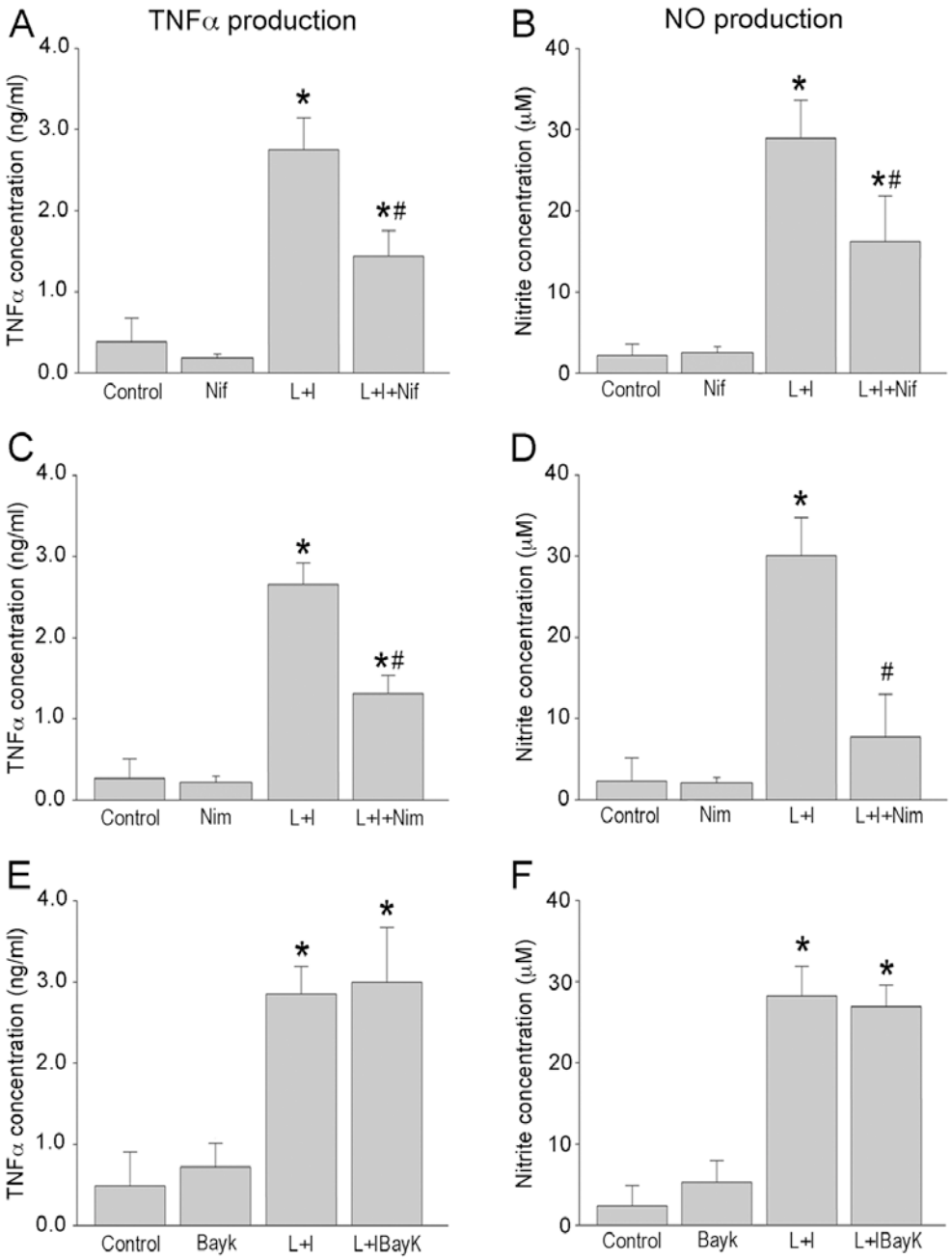

Figure 6: Nifedipine does not modify the phagocytic activity of reactive BV2 microglia.